12270 *J. Phys. Chem. A* **2008,** *112,* 12270–12280

Electronic Structure Studies on Deprotonation of Dithiophosphinic Acids in Water Clusters

Adriana Dinescu and Michael T. Benson*

Idaho National Laboratory, P.O. Box 1625, Idaho Falls, Idaho 83415-2208

Received: July 24, 2008

We report herein a computational study of proton transfer reactions between dithiophosphinic acids (HAs) and water clusters using B3LYP and MP2 methods. The ground-state and transition-state structures of $HA-(H_2O)_n$ ($n = 1, 2, 3$) cluster complexes have been calculated. The influence of water molecules on energy barrier heights of proton transfer reactions has been examined in the gas phase and solution for bis-[*o*-(trifluoromethyl)phenyl]- and bis(2,4,4-trimethylpentyl)dithiophosphinic acids (HA1 and HA2, respectively). Gas-phase calculations indicate that electron-withdrawing substituents and trifluoromethyl groups in the ortho position favor deprotonation of HA1 when three water molecules are included in the cluster. This suggests that at least three water molecules are necessary to solvate the abstracted proton in the presence of the anion. In the case of HA2, the electron-donating groups favor the reverse proton transfer reaction, namely, protonation of dithiophosphinate anion. Bulk solvent effects have been modeled for aqueous and organic media with the CPCM model. The calculated results show that polar solvents can lower the activation energy for less energetically stable transition states that have more localized charges.

Introduction

Owing to the importance and complexity of nuclear waste management, substantial efforts over the past decades have been directed to the separation of actinides (An(III)) from spent nuclear fuel. Effective partitioning of trivalent actinides is affected by the presence of trivalent lanthanides (Ln(III)), which have very similar chemistries and thus give rise to selectivity issues. Among the various extraction systems employed in solvent extraction, dithiophosphinic acids (HAs) are the most promising extractants for selective separation of minor actinides (Am^{3+}, Cm^{3+}) over lanthanides (Eu^{3+}, Gd^{3+}) from aqueous nitric acid solutions.[1] Their selectivity for actinides is most likely controlled by an increase in the metal−ligand bond covalency,[2] on the account of soft−soft interactions between the more diffuse 5f metal orbitals and sulfur donor atoms. The most studied[3] soft-donor extractant is bis(2,4,4-trimethylpentyl)dithiophosphinic acid (commercially available as Cyanex-301). This reagent can selectively extract Am^{3+} over several Ln(III) species, but its susceptibility to chemical decomposition in acidic media may affect the extraction process.[4]

Aromatic dithiophosphinic acids are better extractants than their alkyl counterparts due to the high An(III)/Ln(III) separation factors[5,6] and markedly increased stability[7] that prevents problems associated with radiolytic and hydrolytic degradation. Several aromatic dithiophosphinic acid derivatives[8] have been isolated at the Idaho National Laboratory. Among these, the bis[*o*-(trifluoromethyl)phenyl]dithiophosphinic acid displayed remarkable stability[8a] and very high Am^{3+}/Eu^{3+} separation factors[9] (SF > 10^5) when phenyl trifluoromethyl sulfone (FS-13) was used as a diluent. Although several studies have been published concerning the actinide/lanthanide solvent extraction with bis(2,4,4-trimethylpentyl)dithiophosphinic acid, the transfer of ions between the two phases is not fully understood. It has been recently shown that the liquid−liquid extraction process requires acid deprotonation and metal complexation according to the two-phase equilibrium shown in eq 1.[10]

$$M^{3+}(aq) + 3HA(oil) \rightarrow MA_3(oil) + 3H^+(aq) \qquad (1)$$

Regardless of the mechanistic pathway of reaction 1, acid deprotonation is a key event that is controlled not only by the thermodynamic difference between the reactants and products, but also by the energy barrier associated with the transition state. Quantum mechanical calculations represent a powerful tool in describing the evolution of a system from reactants to products across the transition state, which cannot be captured experimentally. For this reason, we have examined the deprotonation process of HAs from a theoretical perspective using the density functional (DFT)[11] and second-order Møller−Plesset (MP2)[12] theories. Since the relative strength of solvation of species between aqueous and organic solvents is the driving force for the extraction process, solvent effects that govern the acid deprotonation must be considered. Among the available methods, the continuum models[13] offer an effective description of solute−solvent interactions by modeling the solute inside a cavity surrounded by a polarizable continuum medium. It has been shown that single-point free energy solvent corrections using the conductor-like polarizable continuum model (CPCM)[14] generated realistic results for activation barriers of several methyl transfer reactions in aqueous solution.[15] While continuum models are long established in describing the bulk solvent effects, explicit water solvent molecules are necessary for the proton transfer reactions in solution where water can act both as a proton acceptor and/or as a proton donor. This hybrid supermolecule-continuum approach[16] accounts for hydrogen bonding between the solute and nearby water molecules and incorporates the long-range electrostatic interactions with the solvent. Takano et al.[17] found that inclusion of explicit water molecules is necessary for evaluation of activation barriers for hydrolysis of methyl acetate in aqueous solution. They also demonstrated the reliability of CPCM for the computation of the free energy of solvation of organic molecules.

---

* To whom correspondence should be addressed. Phone: (208) 526-1316. Fax: (208) 526-8541. E-mail: Michael.Benson@inl.gov.

10.1021/jp806568k CCC: $40.75

TABLE 1: Gas-Phase Energetics (kcal/mol) for *trans*-HA1 Relative to *cis*-HA1 Using the B3LYP and MP2 Methods[a]

level	ΔE_{el}	ΔE_{ZPE}	ΔH(298.15 K)	ΔG(298.15 K)
B3LYP/6-311G(d,p)	1.01	1.09	1.00	1.65
B3LYP/6-311++G(d,p)	0.72	0.86	0.75	1.31
MP2/6-311++G(d,p)[b]	0.78	0.92	0.81	1.37

[a] Electronic energies (zero-point-exclusive, $\Delta E_{el.}$), zero-point energies (ΔE_{ZPE}), and thermochemical properties (ΔH and ΔG at 298.15 K) are included at different levels of theory. [b] Single-point calculations on the optimized structures at the B3LYP/6-311++G(d,p) level. Thermochemistry corrections are obtained from the B3LYP/6-311++G(d,p) calculations.

The aim of the present work is to study the proton transfer processes in HA−water aggregates by inclusion of up to three explicit water molecules and examine the different microsolvation patterns in terms of structure, thermodynamics, and proton transfer activation barriers in the gas phase and solution. Two dithiophosphinic acids are examined, for which significant experimental work has been carried out: (1) bis[*o*-(trifluoromethyl)phenyl]dithiophosphinic acid (HA1) and (2) bis(2,4,4-trimethylpentyl)dithiophosphinic acid (HA2). Since bis[*o*-(trifluoromethyl)phenyl]dithiophosphinic acid displays higher Am^{3+}/Eu^{3+} separation factors than bis(2,4,4-trimethylpentyl)dithiophosphinic acid,[9] our theoretical work compares the distinct characteristics of these two extractants with regard to proton transfer reactions. To assess the role of the solvent, apart from the aqueous environment, we also consider toluene and FS-13 solvents, as the latter proved to be essential for the extraction of Am(III) with bis[*o*-(trifluoromethyl)phenyl]dithiophosphinic acid.[9]

Computational Methods

Geometry optimizations of ground and transition states, vibrational frequency, intrinsic reaction coordinate (IRC), and self-consistent reaction-field (SCRF) calculations have been carried out with the Gaussian03 suite of programs.[18] Analytic calculations of the energy Hessian confirmed that minimum energy structures have no imaginary frequencies, while transition states are characterized by a single imaginary frequency. Transition-state searches involved the local approach using the Berny optimization algorithm[19] followed by IRC analyses to ensure that two minima are connected along the reaction path through the transition state. Given that Pople-type triple-ζ basis sets are adequate for both neutral and negatively charged sulfur atoms,[20] all calculations have been performed in the gas phase with the widely used[21] B3LYP hybrid density functional[22] and 6-311G(d,p) and 6-311++G(d,p) basis sets. On the basis of a previous study,[23] the 6-311G(d,p) basis offers the best balance between cost and accuracy for proton transfer in malonaldehyde. To reduce errors, however, the current study also considered addition of diffuse functions on hydrogen and heavy atoms as these greatly improve the accuracy of thermochemical calculations.[24] Furthermore, it has been recently reported[25] that Pople-type triple-ζ basis sets with polarization and diffuse functions give the same quality B3LYP results when compared to the more expensive aug-cc-pVTZ Dunning-type basis[26] for a series of hydronium- and hydroxide-containing water clusters. Concerning the performance of the B3LYP functional, one issue may arise from the tendency of gradient-corrected functionals to underestimate reaction barrier heights.[21,27] To benchmark the B3LYP activation energies in the gas phase, single-point calculations at the MP2/6-311++G(d,p) level have been carried out as well. The reason for selecting MP2 lies in its superiority over B3LYP in describing the full range of intermolecular interactions, including dispersion.[28] The geometries and energies have not been corrected for basis set superposition error (BSSE) for several reasons: (1) larger basis sets combined with DFT are expected to generate smaller errors,[29] (2) there is no unique way of correcting the BSSE when more than two fragments compose the aggregate,[30] and (3) the choice of fragments within the transition-state structure can also lead to ambiguities in assessment of the counterpoise correction.[31] Single-point SCRF calculations have been performed on the gas-phase-optimized structures to estimate solvent effects. Solvation corrections to the free energy in aqueous and organic media were obtained for the reactants, products, reactant and product hydrated complexes, and transition structures with the CPCM approach at the B3LYP/6-311++G(d,p) level. As the free energy of solvation is highly dependent upon the solute cavity type, we have employed Pauling radii,[32] as implemented in the Gaussian03 package, on the basis of previous results that involved sulfur-containing species.[15,33] For each CPCM single-point calculation, three solvents have been considered: water, toluene, and FS-13. While for water and toluene we have employed the default parameters (water, dielectric constant $\varepsilon = 78.39$ and solvent radius $r = 1.385$ Å; toluene, dielectric constant $\varepsilon = 2.379$ and solvent radius $r = 2.820$ Å), for the nonstandard FS-13 solvent we have utilized toluene as the predefined solvent with explicitly defined parameters specific for FS-13 (dielectric constant $\varepsilon = 29.0$, solvent radius $r = 3.895$ Å, density $\rho = 0.00404$ molecule/Å^3). All single-point calculations used an SCF energy convergence criterion of 10^{-6} au (SCF=TIGHT).

Results and Discussion

1. Gas-Phase Calculations. All transition- and ground-state geometries have been optimized in the gas phase. The reactant complex and product complex structures have been located along the reaction path by performing IRC calculations. Final IRC geometries have been optimized with B3LYP using both 6-311G(d,p) and 6-311++G(d,p) basis sets. Regardless of the basis set used, B3LYP generated similar geometries. Therefore, the subsequent discussions refer to the B3LYP/6-311++G(d,p)-optimized geometries. To evaluate the microsolvation effect on the activation barrier and thermodynamics properties, we have considered the proton transfer reactions of HA in the presence of water clusters $(H_2O)_n$, $n = 1, 2, 3$, in accordance with eq 2. Optimized geometries of reactant complexes (RCs), transition states (TSs), and product complexes (PCs) with water clusters are denoted on the basis of the number of water molecules (W1, W2, and W3).

$$HA + (H_2O)_n \rightarrow A^- + (H_3O^+)(H_2O)_{n-1} \qquad (2)$$

To test the performance of 6-311G(d,p) and 6-311++G(d,p) basis sets with the B3LYP hybrid functional, we have performed single-point calculations at the MP2/6-311++G(d,p) level. Our results indicate that B3LYP/6-311G(d,p) energy barriers are too low (Tables 2 and 3). Addition of diffuse functions generated superior results for B3LYP that show activation energies closer to those from the MP2 calculations, for one-water and two-water cluster proton transfers. Barrier heights for the three-water cluster aggregates show a lesser agreement between B3LYP/6-311++G(d,p) and MP2/6-311++G(d,p) results. In the latter case, MP2 activation energies are considerably lower than those obtained with B3LYP (deviations in electronic energies for HA−W3 activation barriers range from ~3.5 to 5.5 kcal/mol, dependent on the acid species and reaction mechanism). This is presumably attributable to the BSSE extent in the MP2 results,

TABLE 2: Energies, Enthalpies, and Gibbs Free Energies (kcal/mol) of the HA1−$(H_2O)_n$ RCs, TSs, PCs, and Ps Relative to the Rs at Infinite Separation (BS1:6-311G(d,p), BS2:6-311++G(d,p))

	ΔE_{el}			ΔH(298.15 K)			ΔG(298.15 K)		
	B3LYP		MP2[a]	B3LYP		MP2[a]	B3LYP		MP2[a]
	BS1	BS2	BS2	BS1	BS2	BS2	BS1	BS2	BS2
cis-HA1−W1									
R	0.00	0.00	0.00	0.00	0.00	0.00	0.00	0.00	0.00
RC	−9.50	−6.60	−8.02	−7.97	−5.10	−6.52	0.77	3.75	2.33
TS	−1.54	2.47	2.16	−2.16	1.65	1.34	9.68	13.47	13.16
PC	−10.11	−7.30	−9.06	−8.52	−5.80	−7.56	0.66	3.16	1.4
P	−0.16	−0.36	−0.24	−0.14	−0.30	−0.18	0.04	−0.36	−0.24
trans-HA1−W1									
R	0.00	0.00	0.00	0.00	0.00	0.00	0.00	0.00	0.00
RC	−6.13	−3.31	−5.31	−4.70	−2.01	−4.01	2.76	5.41	3.41
TS	23.80	29.74	30.12	25.24	31.12	31.5	35.88	41.86	42.24
PC	−6.53	−3.16	−5.14	−5.02	−1.90	−3.88	3.35	5.09	3.11
P = R	0.00	0.00	0.00	0.00	0.00	0.00	0.00	0.00	0.00
HA1−W2									
R	0.00	0.00	0.00	0.00	0.00	0.00	0.00	0.00	0.00
RC	−14.80	−10.11	−14.15	−13.15	−8.60	−12.64	0.65	3.39	−0.65
TS	−10.20	−3.60	−5.89	−10.25	−3.60	−5.89	5.47	10.65	8.36
PC	−10.50	−3.74	−6.22	−8.56	−2.10	−4.58	6.90	11.57	9.09
P	109.18	115.68	116.75	109.23	115.48	116.55	112.81	117.73	118.8
HA1−W3a									
R	0.00	0.00	0.00	0.00	0.00	0.00	0.00	0.00	0.00
RC	−9.04	−5.14	−9.98	−8.10	−3.96	−8.80	2.40	6.50	1.65
TS	−6.08	−1.13	−4.94	−7.24	−2.23	−6.04	5.83	11.37	7.56
PC	−13.07	−7.76	−11.99	−11.36	−6.02	−10.25	1.99	7.99	3.76
P	98.30	102.41	103.63	98.32	102.61	103.83	96.25	101.92	103.14
HA1−W3b									
R	0.00	0.00	0.00	0.00	0.00	0.00	0.00	0.00	0.00
RC	−8.19	−6.32	−10.38	−7.27	−5.21	−9.27	2.94	4.60	0.54
TS	15.21	19.96	14.49	16.42	21.33	15.86	29.56	34.82	29.35
PC	−8.68	−3.69	−8.10	−7.25	−2.24	−6.65	5.40	11.14	6.73
P	98.30	102.41	103.63	98.32	102.61	103.83	96.25	101.92	103.14

[a] Single-point calculations on the optimized structures at the B3LYP/6-311++G(d,p) level. Thermochemistry corrections are obtained from the B3LYP/6-311++G(d,p) calculations.

TABLE 3: Energies, Enthalpies, and Gibbs Free Energies (kcal/mol) of the HA2−$(H_2O)_n$ RCs, TSs, PCs, and Ps Relative to the Rs at Infinite Separation (BS1:6-311G(d,p), BS2:6-311++G(d,p))

	ΔE_{el}			ΔH(298.15 K)			ΔG(298.15 K)		
	B3LYP		MP2[a]	B3LYP		MP2[a]	B3LYP		MP2[a]
	BS1	BS2	BS2	BS1	BS2	BS2	BS1	BS2	BS2
HA2−W1									
R	0.00	0.00	0.00	0.00	0.00	0.00	0.00	0.00	0.00
RC	−10.68	−7.18	−9.98	−9.22	−5.67	−8.47	0.44	3.48	0.68
TS	−2.30	1.83	−0.40	−2.93	1.18	−1.05	9.29	13.46	11.23
PC	−10.05	−7.04	−8.96	−8.42	−5.50	−7.42	1.66	3.44	1.52
P	0.16	0.27	0.42	0.10	0.28	0.43	−0.71	−0.70	−0.55
HA2−W2									
R	0.00	0.00	0.00	0.00	0.00	0.00	0.00	0.00	0.00
RC	−14.82	−10.71	−13.20	−13.35	−9.22	−11.71	−0.01	1.95	−0.54
TS	−10.74	−3.71	−5.55	−10.83	−3.53	−5.37	4.88	10.80	8.96
PC	−11.06	−3.73	−5.64	−9.20	−2.42	−4.33	6.47	10.96	9.05
P	114.12	122.17	122.53	114.12	121.99	122.35	117.52	124.52	124.88
HA2−W3									
R	0.00	0.00	0.00	0.00	0.00	0.00	0.00	0.00	0.00
RC	−10.97	−6.60	−10.16	−9.74	−5.23	−8.79	0.46	5.31	1.75
TS	−9.16	−3.48	−6.90	−9.70	−3.95	−7.37	4.02	10.18	6.76
PC	−11.33	−4.94	−8.60	−9.68	−3.19	−6.85	3.43	10.62	6.96
P	103.33	108.90	109.41	103.21	109.12	109.63	100.95	108.71	109.22

[a] Single-point calculations on the optimized structures at the B3LYP/6-311++G(d,p) level. Thermochemistry corrections are obtained from the B3LYP/6-311++G(d,p) calculations.

which is expected to be much larger than BSSE in B3LYP.[34] Another reason for this discrepancy may come from the many-body interactions associated with larger cluster aggregates,[35] which are likely to increase the BSSE even more for the MP2 activation energy of proton transfer reactions in HA−W3 aggregates. Consistent with this effect, our MP2 results show larger deviations from the B3LYP/6-311++G(d,p) results as the size of the aggregate increases from one to three waters.

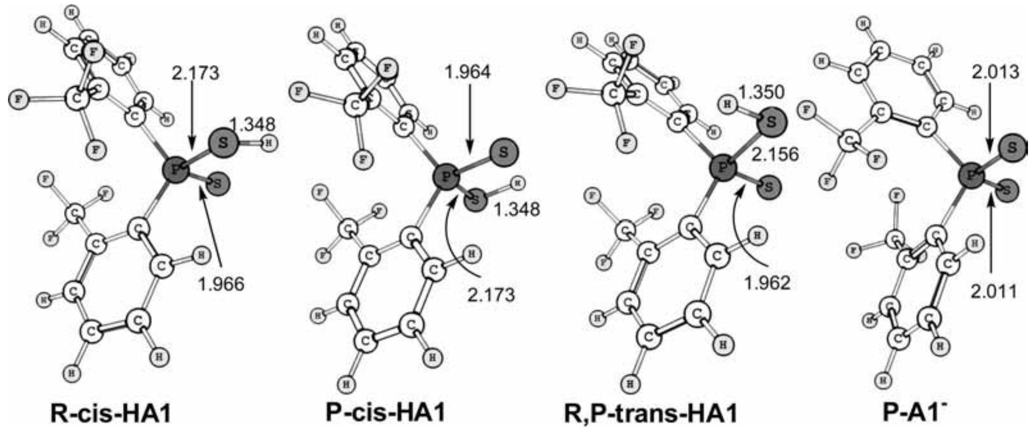

R-cis-HA1 P-cis-HA1 R,P-trans-HA1 P-A1⁻

Figure 1. Optimized structures of HA1 and A1$^-$ at the B3LYP/6-311++G(d,p) level of theory. Selected bond lengths are in angstroms.

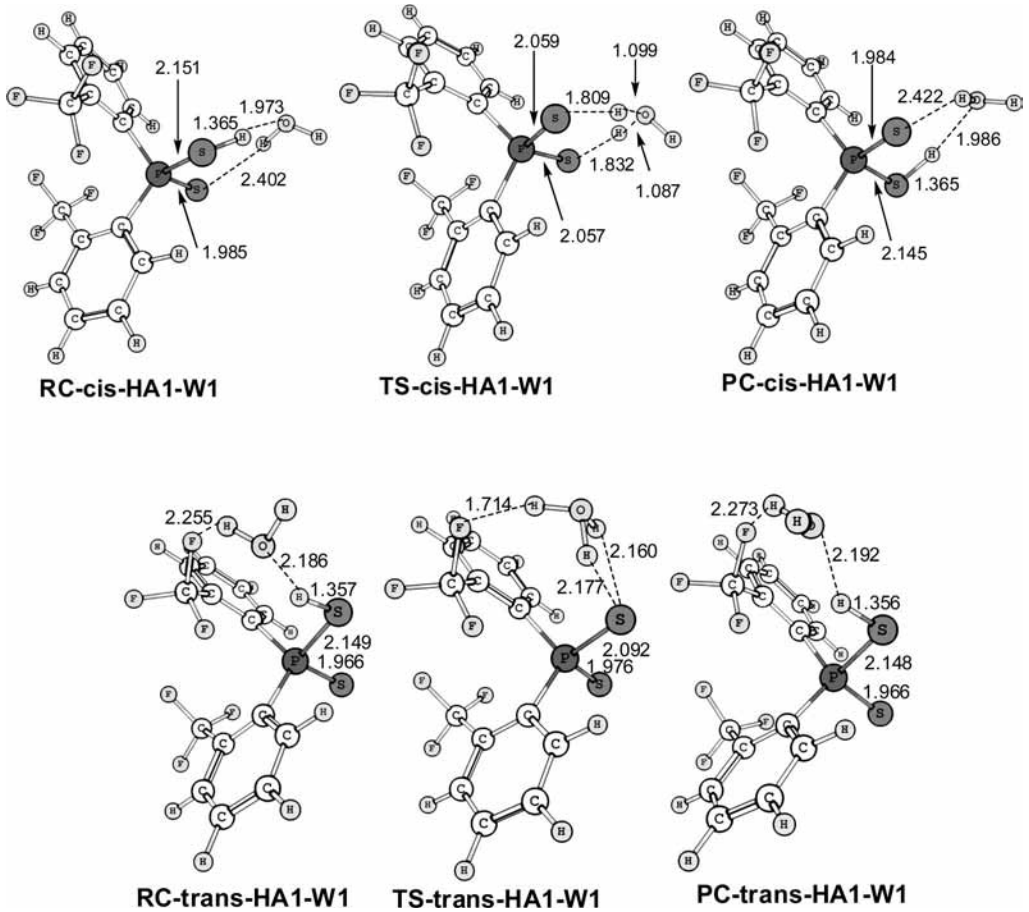

RC-cis-HA1-W1 TS-cis-HA1-W1 PC-cis-HA1-W1

RC-trans-HA1-W1 TS-trans-HA1-W1 PC-trans-HA1-W1

Figure 2. Optimized ground- and transition-state structures of RCs, TSs, and PCs in HA1$-$H$_2$O aggregates using the B3LYP/6-311++G(d,p) method. Selected bond lengths are in angstroms.

On the basis of these observations, we expect B3LYP/6-311++G(d,p) to predict more reliable energies for the systems studied here, when compared to MP2. Further, the triple-ζ quality of the basis set and addition of polarization and diffuse functions are expected to strongly reduce the BSSE magnitude within the DFT formalism.[36] Thus, in the subsequent discussions of energy profiles we refer to the B3LYP/6-311++G(d,p) results.

1.1. Deprotonation of HA1. In Figure 1, the reactant (R) and product (P) represent the neutral (protonated) and anionic structures of HA1. Figures 2$-$4 illustrate the water-assisted proton transfer processes for HA1. We have considered both *cis* and *trans* conformations of the SPS$-$H bond, since the *cis*-HA1 and *trans*-HA1 ground-state energies are separated by only ca. 1 kcal/mol. The relative gas-phase electronic energies (zero-point-exclusive, ΔE_{el}, and zero-point-corrected, ΔE_{ZPE}), enthalpies (ΔH), and Gibbs free energies (ΔG) between *trans* and *cis* conformations of HA1 at different levels of theory are provided in Table 1, whereas their geometries (R-*cis*-HA1 and R,P-*trans*-HA1) are shown in Figure 1. The *trans*-HA1 structure was found to be slightly higher in energy than the *cis*-HA1 geometry. Addition of diffuse functions at the B3LYP level reduces the energy gap between the *trans*- and *cis*-HA1 by approximately 0.3 kcal/mol, this result being consistent with the MP2 energy difference.

For HA1$-$(H$_2$O)$_n$ proton transfer reactions, there are three products (Figure 1), a rearranged *cis*-HA1, where the proton was transferred from the acidic sulfur to the thiophosphoryl

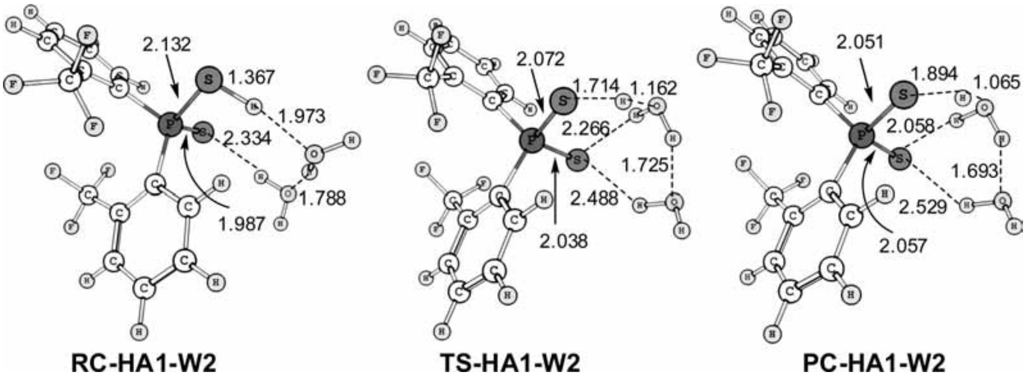

Figure 3. Optimized ground- and transition-state structures of RCs, TSs, and PCs in HA1−$(H_2O)_2$ aggregates using the B3LYP/6-311++G(d,p) method. Selected bond lengths are in angstroms.

sulfur (P-*cis*-HA1), a *trans*-HA1 in which the proton was exchanged, but its structure is identical to the reactant structure (R,P-*trans*-HA1), and a deprotonated anionic species (P-$A1^-$). When compared to R-*cis*-HA1, the P-*cis*-HA1 conformer has a slightly different geometry due to the presence of *o*-(trifluoromethyl)phenyl groups. The steric effects induce an asymmetric orientation of these two groups, which, in turn, gives rise to minor structural and energetic differences between H−SPS and SPS−H conformers.

1.1.1. HA1−H_2O. In the case of one-water cluster models, the proton transfer reactions reveal merely a proton exchange between H_2O and HA1. The transition state involves a double proton transfer reaction, where water simultaneously acts both as a proton acceptor and as a proton donor by mediating two concerted proton transfers. The reaction pathway RC-*cis*-HA1−W1 → TS-*cis*-HA1−W1 → PC-*cis*-HA1−W1 shows the breaking of the S−H bond with formation of the H_3O^+ ion at the transition state and passing on a proton by the H_3O^+ ion to the other sulfur atom (Figure 2). The TS-*cis*-HA1−W1 has a coplanar six-membered ring arrangement with short S−H hydrogen bonds (1.809 and 1.832 Å). For the RC-*trans*-HA1−W1 → TS-*trans*-HA1−W1 → PC-*trans*-HA1−W1 proton transfer reaction (Figure 2), the acidic sulfur is both a proton donor and a proton acceptor, forming a coplanar four-membered ring with the H_3O^+ ion at the transition state. This transition state is additionally stabilized by one short hydrogen bond (1.714 Å) between fluorine and the H_3O^+ ion. The S•••H hydrogen bonds are about 0.3 Å longer in TS-*trans*-HA1−W1 compared to TS-*cis*-HA1−W1. It is worth mentioning that both one-water proton transfer reaction pathways do not result in HA1 deprotonation, but only reflect proton exchange processes.

1.1.2. HA1−$(H_2O)_2$. Calculations for the two-water complex HA1−W2 indicate that the proton is transferred to the water cluster. In this case, the transition state TS-HA1−W2 (Figure 3) has only been found for the *cis*-HA1 reactant conformation. The reaction pathway RC-HA1−W2 → TS-HA1−W2 → PC-HA1−W2 shows the breaking of the S−H bond with formation of the H_3O^+ ion at the transition state (Figure 3). The TS-HA1−W2 geometry indicates a late transition state in which both sulfur atoms hydrogen bond to the H_3O^+ ion while the second water molecule acts as a bridge between the H_3O^+ ion and the non-H-bearing sulfur atom. While the two-water cluster forms two hydrogen bonds with the acid in the RC-HA1−W2 complex, generating an eight-membered ring association, the TS-HA1−W2 and PC-HA1−W2 complexes are each stabilized by three hydrogen bonds, forming two six-membered rings, as shown in Figure 3. Furthermore, the product complex PC-HA1−W2 structure reveals short hydrogen bonds (1.894, 2.058, and 2.529 Å) between the $A1^-$ anion and $H_5O_2^+$ cation, suggesting a strongly bound complex whose geometric arrangement may hinder the metal access in the vicinity of sulfur atoms. The ideal structure of the $H_5O_2^+$ ion is the "Zundel" cation in which the proton is centered between two water molecules. In the PC-HA1−W2 complex, the $H_5O_2^+$ ion has a geometry in which the proton is not equally shared by two waters, but is preferentially bound to the water that abstracts the acidic proton from HA1. Hence, the proton is asymmetrically positioned between a water molecule and the $A1^-$ anion.

1.1.3. HA1−$(H_2O)_3$. Two mechanisms (designated a and b) have been found for the deprotonation of HA1 in the presence of the three-water cluster. The reaction pathways are illustrated by the RC-HA1−W3a → TS-HA1−W3a → PC-HA1−W3a and RC-HA1−W3b → TS-HA1−W3b → PC-HA1−W3b sequences (Figure 4). The reactant complexes and transition-state geometries RC-HA1−W3a, TS-HA1−W3a and RC-HA1−W3b, TS-HA1−W3b (Figure 4) show SPS−H bonds between the *cis*- and *trans*-HA1 conformations. We have also searched for transition states of the *cis*-HA1−W3 conformation, but several attempts finalized at global minima (i.e., no imaginary frequencies). For both mechanisms, the breaking of the S−H bond occurs at the same time with formation of the $H_7O_3^+$ ion. The HA1−W3a mechanism involves a double concerted proton transfer. At TS-HA1−W3a, the acidic SH proton is transferred to the first water molecule, which shuttles its proton toward the second water molecule. All three complexes RC-HA1−W3a, TS-HA1−W3a, and PC-HA1−W3a are characterized by eight-membered ring arrangements with short hydrogen bonds. Structural changes between these complexes are small, suggesting low barrier heights for both forward and reverse reactions. In the PC-HA1−W3a complex, the H_3O^+ ion coordinates to the HA1 conjugate base and two water molecules. The structural arrangement of the $H_3O^+(H_2O)_2$ protonated water cluster is similar to that of the well-known "Eigen" cation in which H_3O^+ forms two short hydrogen bonds (1.571 and 1.585 Å) with the two neighboring water molecules and a third hydrogen bond with the conjugate base of HA1. The HA1−W3b mechanism involves only a single proton transfer. The acidic SH proton is first abstracted by the water molecule that hydrogen bonds to the fluorine atom and then is transferred to the neighboring water molecule, thereby producing a H_3O^+ ion coordinated to two water molecules. Transition from RC-HA1−W3b to TS-HA1−W3b involves rotation of the water molecule that initially abstracts the acidic proton, while transition from TS-HA1−W3b to PC-HA1−W3b involves rotation of the next water molecule to which the proton is eventually transferred. In the RC-HA1−W3b complex, there are two hydrogen bonds (1.858 and 2.338 Å) between HA1 and the three-water cluster, generating a 10-membered ring arrangement. Structural

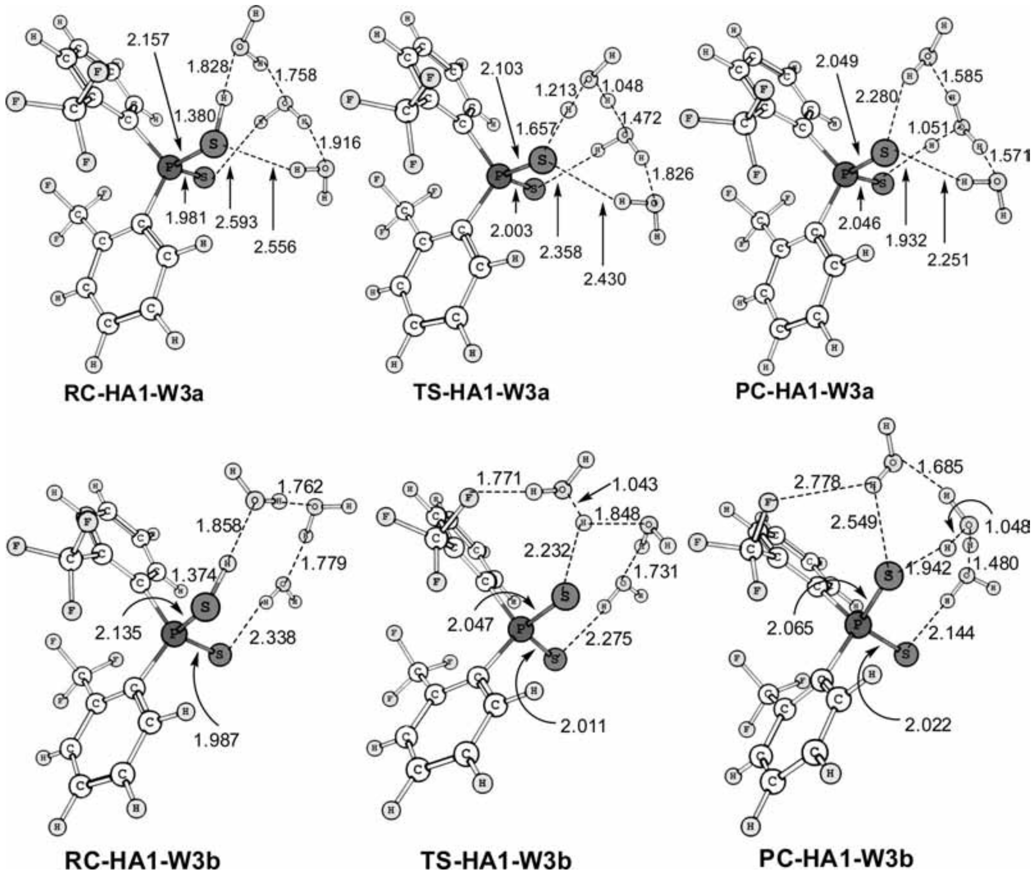

Figure 4. Optimized ground- and transition-state structures of RCs, TSs, and PCs in HA1−$(H_2O)_3$ aggregates using the B3LYP/6-311++G(d,p) method. Selected bond lengths are in angstroms.

changes from RC-HA1−W3b to TS-HA1−W3b show that one inside hydrogen bond (1.762 Å) belonging to the water cluster is broken and two new hydrogen bonds (1.771 and 1.848 Å) are formed, producing a distorted eight-membered ring and an outer water molecule that hydrogen bonds to the fluorine atom. The PC-HA1−W3b complex holds one eight-membered ring and one six-membered ring. Structural changes indicate that one hydrogen bond (2.232 Å) is broken and two new hydrogen bonds (1.942 and 2.549 Å) are formed in the product complex. The structural changes within the HA1−W3b mechanism reflect an increase of the number of hydrogen bonds from two to three in the transition state, which can be attributed to the presence of the fluorine atom near the acidic proton. This means that the *o*-trifluoromethyl substituent is favorably located so that it participates in transition-state stabilization. Thus, in addition to its electron-withdrawing feature, the *o*-trifluoromethyl group facilitates the deprotonation of the HA1 acid by hydrogen bonding. Also, the optimized geometry of the product complex suggests that adequate space exists for a metal cation to coordinate to the sulfur atoms.

Noteworthy, for both the HA1−W3a and HA1−W3b mechanisms, the geometrical arrangement of the $H_3O^+(H_2O)_2$ ion in the product complex (hydronium ion coordinated to two water molecules) is similar to that previously reported[37] to be the lowest energy conformation.

1.1.4. Gas-Phase Energies. The energies of the HA1−$(H_2O)_n$ RCs, TSs, and PCs relative to the Rs are listed in Table 2. The electronic energy (zero-point-exclusive), ΔE_{el}, enthalpy, ΔH, at 298.15 K, and Gibbs free energy, ΔG, at 298.15 K, have been included. Although our discussions will mostly refer to ΔG, its value is strongly dependent on the calculated vibrational frequency values, thereby being less accurate than ΔH or ΔE. For this reason, all three values need to be considered when the results are interpreted. In the gas phase all water-assisted proton transfer reactions go through the formation of the RC and PC, whose enthalpies are lower than the sum of the enthalpies of the reactants, but whose free energies are higher relative to those of the reactants. The activation barriers for *cis*-HA1−W1, HA1−W2, and HA1−W3a reactions are much lower than the activation barriers for *trans*-HA1−W1 and HA1−W3b reactions. This is consistent with the extent of transition-state stabilization by hydrogen bonding between the negatively charged sulfur atoms and water molecules. Stronger hydrogen bonds at the transition state result in lower activation energies.

As mentioned above, we discuss the results obtained with the B3LYP/6-311++G(d,p) level of theory. The calculated activation barrier for the one-water-assisted proton transfer between the two sulfur atoms of *cis*-HA1−W1 (Table 2) is fairly low ($\Delta G^{\ddagger} = 13.16$ kcal/mol). This suggests a rapid equilibrium between the reactants and products and, thus, contrasts with the free energy activation barrier for *trans*-HA1-W1 single-water proton transfer, which is significantly higher ($\Delta G^{\ddagger} = 41.86$ kcal/mol). This is likely caused by *cis*-HA1 passing through a nearly coplanar six-membered ring transition state, while *trans*-HA1 involves a four-membered ring transition state that is expected to be less energetically favored due to the large angle strain.

The two-water-cluster-assisted proton transfer reaction (Table 2, *cis*-HA1−W2) is highly endothermic in the gas phase and has a calculated free energy barrier of only 10.65 kcal/mol. The reason for this low barrier height lies in the structure of the transition state, which is stabilized by a larger number of solute−solvent hydrogen bonds than the reactant complex. Surprisingly, the free energy of the product complex is slightly higher than that of the transition state by 0.92 kcal/mol, whereas

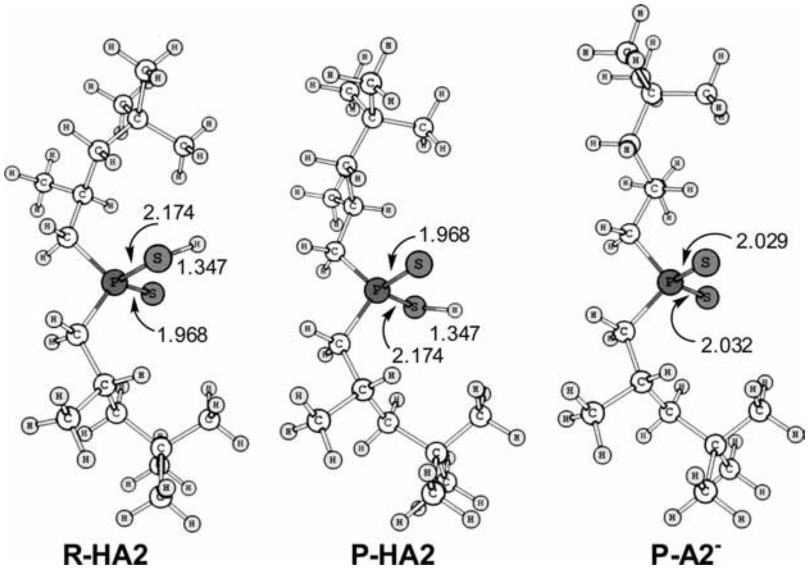

Figure 5. Optimized structures of HA2 and $A2^-$ at the B3LYP/6-311++G(d,p) level of theory. Selected bond lengths are in angstroms.

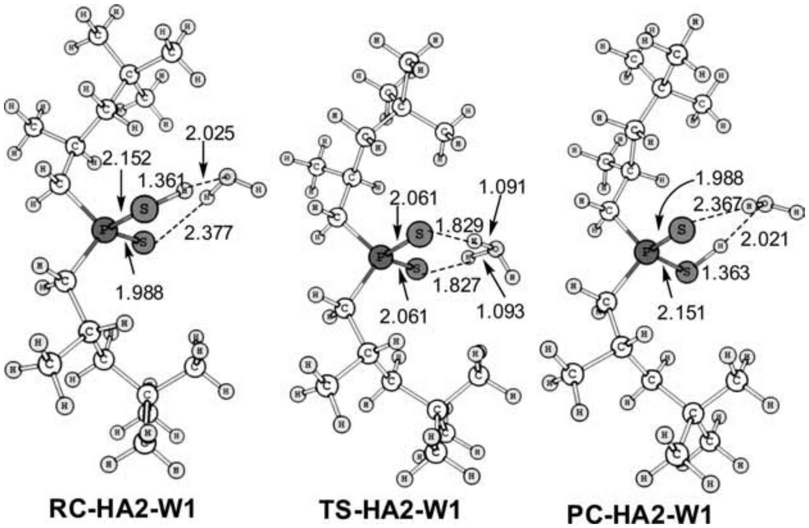

Figure 6. Optimized ground- and transition-state structures of $HA2-H_2O$ aggregates using the B3LYP/6-311++G(d,p) method. Selected bond lengths are in angstroms.

the reactant complex rests 7.26 kcal/mol lower than the transition state. This result could be attributed to the optimization algorithm, which searches for stationary points on the basis of electronic energies rather than free energies. Nevertheless, the electronic energy of the product complex is only 0.14 kcal/mol lower than that of the transition state, but still significantly higher than that of the reactant complex by 6.37 kcal/mol. Thus, the two-water cluster deprotonation of HA1 results in a short-lived product complex species, since the reverse reaction is essentially barrierless and overall equilibrium would rather proceed toward the reactants.

The free energy barriers for the three-water-cluster-assisted proton transfer are 11.37 and 34.82 kcal/mol for the HA1−W3a and HA1−W3b mechanisms, respectively (Table 2). While these barriers are higher than that associated with the two-water cluster (by 0.72 and 24.17 kcal/mol, respectively), the product complex is significantly lower in energy than the transition state in both cases. This is because the hydronium ion, as discussed above, is solvated by two water molecules and the anion$-H_7O_3^+$ ion pair is better stabilized through hydrogen bonding. The dissociation reaction is still highly endothermic, but the structure and favorable energy of the product complex indicate that deprotonation of HA1 is feasible in the presence of three-water clusters. The high activation energy (34.82 kcal/mol) for the HA1−W3b mechanism is consistent with the large structural changes at the transition state, and although this barrier is higher than that for the HA1−W3a mechanism, we need to consider the HA1−W3b mechanism as a possible reaction pathway in solution.

1.2. Deprotonation of HA2. In Figure 5, R and product P represent the neutral (protonated) and anionic structures of HA2. Water-assisted proton transfer processes for HA2 are illustrated in Figures 6−8. Similar to the previous section, $HA2-(H_2O)_n$ aggregates relevant to the reaction coordinate have been optimized, and selected bond distances obtained at the B3LYP/6-311++G(d,p) level are given in the figures.

1.2.1. $HA2-H_2O$ and $HA2-(H_2O)_2$. The one-water- and two-water-assisted proton transfer reactions, denoted RC-HA2−W1 → TS-HA2−W1 → PC-HA2−W1 (Figure 6) and RC-HA2−W2 → TS-HA2−W2 → PC-HA2−W2 (Figure 7), respectively, show structural patterns very similar to those seen for HA1. However, due to the presence of the branched alkyl chains, only the *cis* conformation of HA2 is accessible. The one-water-assisted proton transfer reaction reveals a concerted

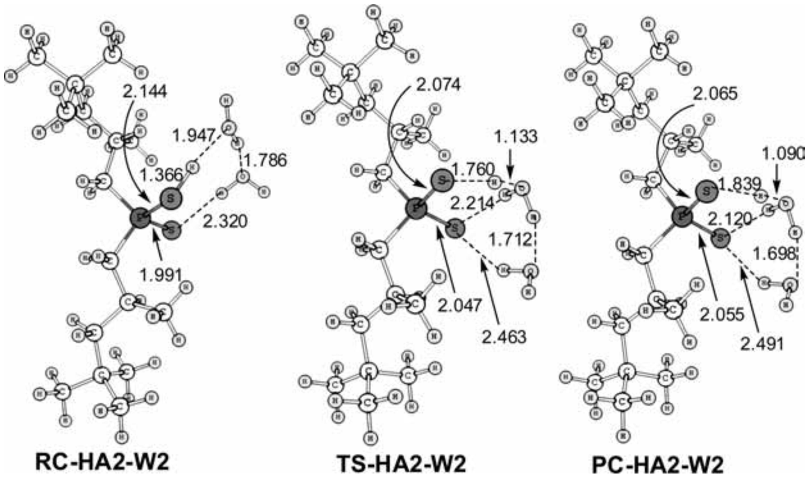

Figure 7. Optimized ground- and transition-state structures of HA2−$(H_2O)_2$ aggregates using the B3LYP/6-311++G(d,p) method. Selected bond lengths are in angstroms.

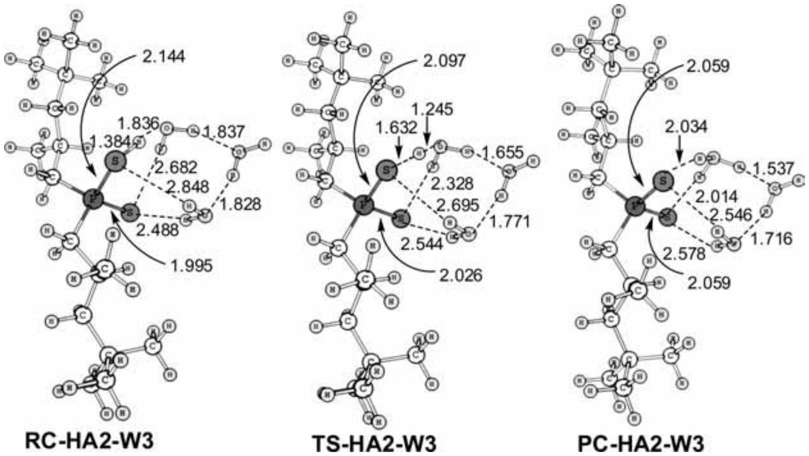

Figure 8. Optimized ground- and transition-state structures of HA2−$(H_2O)_3$ aggregates using the B3LYP/6-311++G(d,p) method. Selected bond lengths are in angstroms.

double proton exchange between the water molecule and the two sulfur atoms by passing through a six-membered ring transition state (Figure 6) as seen in HA1. Again, this reaction does not deprotonate HA2, but only exchanges the proton with water. Addition of a second water leads to a reaction pathway in which the proton shuttles back and forth between the acidic sulfur and one of the water molecules. The two-water cluster transition state TS-HA2−W2 upholds the six-membered ring arrangement with further hydrogen bonding between the non-H-bearing sulfur and the second water molecule. Similar to the HA1−W2 mechanism, after the HA2 proton is transferred to the first water molecule, the protonated water cluster $H_5O_2^+$ does not reach the energetically favored conformation where the proton is equally shared by two water molecules. Instead, the well-defined H_3O^+ moiety of the $H_5O_2^+$ cluster forms hydrogen bonds with the dithiophosphinate anion and the second water molecule (Figure 7).

1.2.2. HA2−$(H_2O)_3$. While proton transfers to one-water and two-water clusters in HA2 aggregates display pathways very similar to those calculated for HA1, this is not the case with the three-water cluster. The corresponding reaction pathway RC-HA2−W3 → TS-HA2−W3 → PC-HA2−W3 is given in Figure 8. In contrast with the results obtained for HA1, the transition state of HA2 with the three-water cluster (TS-HA2−W3) is predominantly the transition state of HA2 with the two-water cluster (TS-HA2−W2) that adds in an extra water molecule. Hence, the hydronium ion is strongly bound to the $A2^-$ anion in both the transition state and product complex, preventing proton migration inside the water cluster. In essence, all three transition states TS-HA2−W1, TS-HA2−W2, and TS-HA2−W3 are dominated by short hydrogen bonds between the acid anion and H_3O^+ unit. Our attempt to solvate the proton to form an Eigen cation, by modeling the four-water-assisted proton transfer, resulted in a transition state with the same pattern; i.e., the H_3O^+ ion coordinates to the two sulfur atoms, and the proton does not migrate to the next water molecule. This can be explained by an increased negative charge on the sulfur centers in the anion due to the presence of electron-donating substituents (two 2,4,4-trimethylpentyl groups). As a consequence, the H_3O^+ cation will interact stronger with the $A2^-$ anion than with the water cluster. A more detailed comparative analysis concerning microsolvation of HA1 and HA2 by a three-water cluster is provided in a separate section below.

1.2.3. Gas-Phase Energies. To test the validity of our energy computations, we have employed the same three levels of theory, B3LYP/6-311G(d,p), B3LYP/6-311++G(d,p), and MP2/6-311++G(d,p), as for HA1−water aggregates (vide supra). The energies for calculated stationary points relative to reactants are summarized in Table 3. On the basis of considerations mentioned earlier, B3LYP/6-311++G(d,p) results are preferred for chemical systems of this type. The calculated free energy activation barriers for the proton transfer in HA2−water aggregates are low, and little variation occurs with respect to the water cluster size ($\Delta G^{\ddagger}$ ranges from 13.46 to 10.18 kcal/

mol at the B3LYP/6-311++G(d,p) level). These low barriers are consistent with gas-phase transition-state geometries, which show formation of short cyclic hydrogen bonds connecting charged fragments (Figures 5−7). Comparing the energies for one-water and two-water cluster proton transfers, the barrier height is reduced by 2.66 kcal/mol by the presence of the second water molecule. However, inclusion of a third water molecule has a negligible effect relative to that of the two-water cluster, lowering the free activation energy by only 0.62 kcal/mol. This is because the transition-state structures TS-HA2−W2 and TS-HA2−W3 are very similar, both involving single proton transfers with similar hydrogen-bonding patterns between the acid anion and H_3O^+ ion, as already explained.

1.3. Comparison between Aggregates of HA1 and HA2 with $(H_2O)_3$. As far as the differences between HA1−$(H_2O)_3$ and HA2−$(H_2O)_3$ are concerned, TS-HA2−W3 (Figure 8) is dominated by a larger number of hydrogen bonds than TS-HA1−W3a or TS-HA1−W3b (Figure 4). The bulky 2,4,4-trimethylpentyl substituents of HA2 constrain the arrangement of water molecules around the sulfur atoms. Also, the electron-donating effect of the alkyl group increases the negative partial charge on the sulfurs (natural charges are given in the Supporting Information), which in turn strengthens the hydrogen bonding between the anion and protonated water cluster. TS-HA2−W3, where the H_3O^+ ion is strongly bound to the dithiophosphinate $A2^-$ anion, is energetically stabilized by hydrogen bonding (Figure 8), preventing further proton transfer to the next water molecule inside the water cluster and thus favoring the reverse reaction. In contrast with the HA2−$(H_2O)_3$ aggregate, the two pathways for HA1−$(H_2O)_3$ proton transfer lead to formation of a stable protonated water cluster (H_3O^+ bonded to two water molecules, Figure 4). The reaction pathway for TS-HA1−W3a involves a concerted double proton transfer. Once the acidic proton is transferred from HA1 to a neighboring water molecule, this molecule generates a short hydrogen bond to the second water molecule and shuttles its hydrogen-bonded proton to the middle water to form a stable $H_7O_3^+$ protonated water cluster. On the other hand, TS-HA1−W3b shows a single proton transfer that leads to rotation of the first water molecule inside the cluster. This water molecule abstracts the acidic proton and rotates to form a hydrogen bond with the fluorine. Additionally, the rotation of the first water in the cluster facilitates the further transfer of the acidic proton to the second water molecule, leading to a stable $H_7O_3^+$ protonated water cluster. The larger structural changes and longer distance covered by the acidic proton along the HA1−W3b reaction pathway are reflected in the higher energy of activation (Table 2).

To extend the present calculations to include more explicit water molecules is beyond the scope of this study, as it would require an in-depth analysis, mostly because of the conformational diversity of HA1−$(H_2O)_n$ aggregates ($n > 3$). Nevertheless, the effect of bulk solvation can be estimated using a continuum model. Typically, the hybrid cluster-continuum approaches represent an improvement over the continuum models for prediction of free energies of solvation.[16,38] Hence, we have employed this approach to examine the solvent effects on the proton transfer in dithiophosphinic acid−water clusters.

2. Solvent-Phase Calculations. The CPCM single-point calculations have been applied at the B3LYP/6-311++G(d,p) level to all ground- and transition-state geometries listed in Tables 2 and 3. The free energies in solution for reactants, reactant complexes, transition states, product complexes, and products relative to reactants in the gas phase have been estimated as the sum of the gas-phase free energies relative to those of the reactants and the solvation contribution to the free energy for each chemical species. To better exploit the CPCM formalism, we have included both electrostatic and nonelectrostatic components of the free energy of solvation. Solvent-corrected free energies of stationary points relevant to deprotonation of HA1 and HA2 in water, toluene, and FS-13 are given in Table 4. The free energies of activation ($\Delta G^\ddagger$) and free energies of reaction (ΔG_{rxn}) in the gas phase and solution are also estimated.

In the case of one-water-assisted proton transfer, all three solvents increase the activation barriers for both *cis*-HA1-W1 and HA2−W1 species compared to the gas-phase results (Table 4). This is due to the reactants being more strongly solvated than the transition states. The calculated results suggest that using toluene could lead to slightly lower barriers than using water or FS-13 solvents, corresponding to a less solvated reactant in toluene. Interestingly, solvent-corrected activation energies for *cis*-HA1−W1 are approximately 2−3 kcal/mol lower than those for HA2−W1 ($\Delta\Delta G^\ddagger$ differences in water, toluene, and FS-13 are 3.1, 1.7, and 2.9 kcal/mol, respectively), even though the gas-phase barrier heights are the same ($\Delta G^\ddagger = 13.5$ kcal/mol). This is presumably caused by the large differences between HA1 and HA2 in terms of their solvation energies. For the *trans*-HA1−W1 proton transfer, the solvent-corrected activation barriers in water, toluene, and FS-13 are still dominated by the large gas-phase barrier height ($\Delta G^\ddagger = 41.9$ kcal/mol), but are lower than in the gas phase by ca. 2−6 kcal/mol. In this case the transition state is more strongly solvated than the reactants. It appears that structural arrangement of the transition state TS-*trans*-HA1−W1 (Figure 2), in which only one of the two sulfur atoms hydrogen bonds to the H_3O^+ ion, leads to more negative solvation energy, especially in polar solvents, i.e., water and FS-13. This is consistent with gas-phase natural charges, which show a significant variance between the two sulfur atoms (natural charges are −0.5 for the hydrogen-bonded sulfur and −0.7 for the other) and hence indicate that the excess of negative charge is stabilized by a polar solvent.

The two-water-assisted proton transfer energy barriers for HA1−W2 and HA2−W2 (Table 4) show almost identical values, most likely due to very similar structural patterns of the transition states. The solvent-corrected activation energies are higher than the gas-phase energies as a result of better solvated reactants than transition states. Similar to the one-water results, the lowest barrier height is obtained in toluene on account of the less favorable solvation energy for reactants in toluene compared to water or FS-13.

In the case of three-water deprotonation of HA1 according to the HA1−W3a mechanism, applying solvent correction increases the activation barrier (Table 4) due to the same reason stated above: reactants are more strongly solvated than the transition state. Solvent effects for deprotonation of HA1 in the presence of three-water clusters according to the HA1−W3b mechanism have little influence on barrier heights because of comparable solvation energies of the reactants and transition state (Table 4). However, the FS-13 solvent yields a lower energy barrier than toluene by 3.1 kcal/mol. In this case, it appears that FS-13 provides the most favorable energy balance between the reactants and transition state, by solvating the transition state more strongly than the reactants. For HA2 deprotonation in the presence of a three-water cluster, we have found one mechanism. Since the three-water deprotonation of HA2 follows a pattern very similar to that of the two-water deprotonation, barrier heights are almost identical in both the

TABLE 4: Gas-Phase and Solvent-Corrected[a] Gibbs Free Energies (kcal/mol) of the Rs, RCs, TSs, PCs, and Ps Relative to the Reactants in the Gas Phase, Calculated with B3LYP/6-311++G(d,p)[b]

	HA1				HA2			
	gas phase	water	toluene	FS-13	gas phase	water	toluene	FS-13
	cis-HA1-W1				HA2-W1			
R	0.00	−11.26	−3.08	−5.55	0.00	12.51	14.56	14.47
RC	3.75	−0.39	4.83	4.57	3.48	25.43	23.83	26.67
TS	13.47	5.74	12.49	11.15	13.46	32.56	31.83	34.05
PC	3.16	−0.83	4.41	4.15	3.44	24.24	22.97	25.63
P	−0.12	−11.74	−3.40	−5.77	−0.70	11.27	13.49	13.21
$\Delta G^{\ddagger}$	13.47	17.00	15.57	16.70	13.46	20.05	17.27	19.58
ΔG_{rxn}	−0.12	−0.48	−0.32	−0.22	−0.70	−1.24	−1.07	−1.26
	HA1-W2				HA2-W2			
R	0.00	−16.51	−5.72	−10.14	0.00	7.26	11.92	9.88
RC	3.39	−0.39	5.32	4.60	1.95	20.21	20.64	21.95
TS	10.65	4.71	11.32	10.51	10.80	29.12	29.37	31.47
PC	11.57	4.87	12.03	10.92	10.96	28.94	29.27	31.37
P	117.73	−6.20	50.21	3.59	124.52	20.47	72.65	28.32
$\Delta G^{\ddagger}$	10.65	21.22	17.04	20.65	10.80	21.86	17.45	21.59
ΔG_{rxn}	117.73	10.31	55.93	13.73	124.52	13.21	60.73	18.44
	HA1-W3a				HA2-W3			
R	0.00	−14.99	−4.79	−8.37	0.00	8.78	12.85	11.65
RC	6.50	1.06	8.87	7.16	5.31	24.78	25.30	26.71
TS	11.37	3.39	11.79	9.37	10.18	29.60	29.76	31.60
PC	7.99	0.78	8.75	6.81	10.62	28.52	29.41	30.89
P	101.92	−12.40	40.35	−1.74	108.71	14.27	62.79	22.99
$\Delta G^{\ddagger}$	11.37	18.38	16.58	17.74	10.18	20.82	16.91	19.95
ΔG_{rxn}	101.92	2.59	45.14	6.63	108.71	5.49	49.94	11.34
	HA1-W3b				trans-HA1-W1			
R	0.00	−14.99	−4.79	−8.37	0.00	−11.52	−3.11	−5.75
RC	4.60	−1.73	6.29	3.91	5.41	0.15	6.50	5.50
TS	34.82	18.16	30.98	24.27	41.86	24.77	37.02	31.18
PC	11.14	2.74	11.42	8.71	5.09	−0.04	6.38	5.30
P	101.92	−12.40	40.35	−1.74	0.00	−11.52	−3.11	−5.75
$\Delta G^{\ddagger}$	34.82	33.15	35.77	32.64	41.86	36.29	40.13	36.93
ΔG_{rxn}	101.92	2.59	45.14	6.63	0.00	0.00	0.00	0.00

[a] Single-point CPCM-B3LYP/6-311++G(d,p) calculations on the optimized structures at the B3LYP/6-311++G(d,p) level. [b] Free energy activation barriers and reaction free energies are given for both the gas and solvent phases.

gas phase and solution, but the three-water cluster gives slightly lower barriers by ca. 0.5 kcal/mol (HA2−W3, Table 4).

Conclusions

We have examined the role of microsolvation on energy barriers for the deprotonation of two dithiophosphinic acids, HA1 and HA2, and explored the bulk solvent effects of water, toluene, and FS-13. A series of quantum mechanical calculations have been carried out based on the hybrid supermolecule-continuum approach, in which up to three solvent water molecules are explicitly included in the supermolecular reaction coordinate calculations and the bulk solvent is modeled as a polarizable dielectric continuum. We have found that adding explicit waters from one to two molecules lowers the activation energy for both HA1 and HA2 deprotonation processes by ca. 3 kcal/mol, while adding a third molecule generates different trends between HA1 and HA2. For HA1 deprotonation, addition of a third water molecule raises the barrier height by ca. 1 or 24 kcal/mol in the gas phase, depending on the reaction pathway. For HA2 deprotonation, addition of a third water molecule lowers the barrier height by ca. 1 kcal/mol. These results are consistent with the extent of hydrogen bonding at the transition state. Stronger hydrogen bonds between solute and water molecules lower the activation energies as a result of stabilization of charges.

It is worth mentioning that our results suggest that at least three water molecules are needed to completely deprotonate HA1, which leads to formation of a stable protonated water cluster. Two reaction pathways, HA1−W3a and HA1−W3b, have been found for HA1−$(H_2O)_3$ proton transfer. While the barrier for the HA1−W3b pathway is less favorable than for the HA1−W3a pathway by ca. 23 kcal/mol, this higher barrier is still feasible, particularly when we consider the structural arrangement of the transition state that would provide enough room for a metal cation to bind to the negatively charged sulfur atoms. It is likely that the presence of a metal cation in the vicinity of sulfur atoms would counterbalance their negative charge and thus lower the proton transfer barrier height associated with the HA1−W3b pathway. Furthermore, deprotonation of HA1 in the presence of a three-water cluster results in energetically stable product complexes for both pathways. In the case of three-water-assisted deprotonation of HA2, the barrier height is very low ($\Delta G^{\ddagger} = 10.18$ kcal/mol), but the product complex is energetically unstable relative to the transition state, suggesting the deprotonated species is short-lived.

Accounting for bulk solvent effects seems more important when the gas-phase barrier heights are low, and more negative solvation energies of the reactants substantially contribute to raising the activation energies. For higher gas-phase activation barriers, including bulk solvent effects is less important due to similar solvation energies of the reactants and transition states. Nevertheless, polar solvents, such as water and FS-13, stabilize the transition states more than the reactants when charges are more delocalized (HA1−W3b and trans-HA1−W1 pathways).

Acknowledgment. This work was supported by the U.S. Department of Energy (DOE), INL Laboratory Directed Research & Development Program, under DOE Idaho Operations Office Contract DE-AC07-05ID14517.

Supporting Information Available: Natural charges and Cartesian coordinates of optimized geometries of the reactants, products, transition states, reactant complexes, and product complexes. This material is available free of charge via the Internet at http://pubs.acs.org.

References and Notes

(1) Mathur, J. N.; Murali, M. S.; Nash, K. L. *Solvent Extr. Ion Exch.* **2001**, *19*, 357–390.

(2) Jensen, M. P.; Bond, A. H. *J. Am. Chem. Soc.* **2002**, *124*, 9870–9877.

(3) (a) Zhu, Y. *Radiochim. Acta* **1995**, *68*, 95–98. (b) Zhu, Y.; Chen, J.; Jiao, R. *Solvent Extr. Ion Exch.* **1996**, *14*, 61–68. (c) Zhu, Y.; Chen, J.; Choppin, G. R. *Solvent Extr. Ion Exch.* **1996**, *14*, 543–553. (d) Ionova, G.; Ionov, S.; Rabbe, C.; Hill, C.; Madic, C.; Guillaumont, R.; Krupa, J. C. *Solvent Extr. Ion Exch.* **2001**, *19*, 391–414. (e) Jensen, M. P.; Chiarizia, R.; Urban, V. *Solvent Extr. Ion Exch.* **2001**, *19*, 865–884. (f) Tian, G.; Zhu, Y.; Xu, J.; Zhang, P.; Hu, T.; Xie, Y.; Zhang, J. *Inorg. Chem.* **2003**, *42*, 735–741. (g) Tian, G.; Kimura, T.; Yoshida, Z.; Zhu, Y.; Rao, L. *Radiochim. Acta* **2004**, *92*, 495–499. (h) Bhattacharyya, A.; Mohapatra, P. K.; Manchanda, V. K. *Solvent Extr. Ion Exch.* **2007**, *25*, 27–39.

(4) Law, J. D.; Peterman, D. R.; Todd, T. A.; Tillotson, R. D. *Radiochim. Acta* **2006**, *94*, 261–266.

(5) Modolo, G.; Odoj, R. *Solvent Extr. Ion Exch.* **1999**, *17*, 33–53.

(6) Modolo, G.; Nabet, S. *Solvent Extr. Ion Exch.* **2005**, *23*, 359–373.

(7) Modolo, G.; Seekamp, S. *Solvent Extr. Ion Exch.* **2002**, *20*, 195–210.

(8) (a) Klaehn, J. R.; Peterman, D. R.; Harrup, M. K.; Tillotson, R. D.; Luther, T. A.; Greenhalgh, M. R.; Law, J. D.; Daniels, L. D. *Inorg. Chim. Acta* **2008**, *361*, 2522–2532. (b) Leavitt, C. M.; Gresham, G. L.; Benson, M. T.; Gaumet, J.-J.; Peterman, D. R.; Klaehn, J. R.; Moser, M.; Aubriet, F.; Van Stipdonk, M. J.; Groenewold, G. S. *Inorg. Chem.* **2008**, *47*, 3056–3064. (c) Klaehn, J. R.; Peterman, D. R.; Harrup, M. K.; Tillotson, R. D.; Luther, T. A.; Greenhalgh, M. R.; Law, J. D.; Daniels, L. D. *234th ACS National Meeting*, Boston, MA, Aug 19−23, 2007; American Chemical Society: Washington, DC, 2007; INOR-964.

(9) Peterman, D. R.; Greenhalgh, M. R.; Tillotson, R. D.; Klaehn, J. R.; Harrup, M. K.; Luther, T. A.; Law, J. D.; Daniels, L. D. *234th ACS National Meeting*, Boston, MA, Aug 19−23, 2007; American Chemical Society: Washington, DC, 2007; INOR-539.

(10) Jensen, M. P.; Bond, A. H. *Radiochim. Acta* **2002**, *90*, 205–209.

(11) Kohn, W.; Becke, A. D.; Parr, R. G. *J. Phys. Chem.* **1996**, *100*, 12974–12980.

(12) Møller, C.; Plesset, M. S. *Phys. Rev.* **1934**, *46*, 618–622.

(13) Tomasi, J.; Mennucci, B.; Cammi, R. *Chem. Rev.* **2005**, *105*, 2999–3093.

(14) Barone, V.; Cossi, M. *J. Phys. Chem. A* **1998**, *102*, 1995–2001.

(15) Gunaydin, H.; Acevedo, O.; Jorgensen, W. L.; Houk, K. N. *J. Chem. Theory Comput.* **2007**, *3*, 1028–1035.

(16) (a) Pliego, J. R.; Riveros, J. M. *J. Phys. Chem. A* **2001**, *105*, 7241–7247. (b) Pliego, J. R.; Riveros, J. M. *J. Phys. Chem. A* **2002**, *106*, 7434–7439.

(17) Takano, Y.; Houk, K. N. *J. Chem. Theory Comput.* **2005**, *1*, 70–77.

(18) Frisch, M. J.; Trucks, G. W.; Schlegel, H. B.; Scuseria, G. E.; Robb, M. A.; Cheeseman, J. R.; Montgomery, J. A., Jr.; Vreven, T.; Kudin, K. N.; Burant, J. C.; Millam, J. M.; Iyengar, S. S.; Tomasi, J.; Barone, V.; Mennucci, B.; Cossi, M.; Scalmani, G.; Rega, N.; Petersson, G. A.; Nakatsuji, H.; Hada, M.; Ehara, M.; Toyota, K.; Fukuda, R.; Hasegawa, J.; Ishida, M.; Nakajima, T.; Honda, Y.; Kitao, O.; Nakai, H.; Klene, M.; Li, X.; Knox, J. E.; Hratchian, H. P.; Cross, J. B.; Bakken, V.; Adamo, C.; Jaramillo, J.; Gomperts, R.; Stratmann, R. E.; Yazyev, O.; Austin, A. J.; Cammi, R.; Pomelli, C.; Ochterski, J. W.; Ayala, P. Y.; Morokuma, K.; Voth, G. A.; Salvador, P.; Dannenberg, J. J.; Zakrzewski, V. G.; Dapprich, S.; Daniels, A. D.; Strain, M. C.; Farkas, O.; Malick, D. K.; Rabuck, A. D.; Raghavachari, K.; Foresman, J. B.; Ortiz, J. V.; Cui, Q.; Baboul, A. G.; Clifford, S.; Cioslowski, J.; Stefanov, B. B.; Liu, G.; Liashenko, A.; Piskorz, P.; Komaromi, I.; Martin, R. L.; Fox, D. J.; Keith, T.; Al-Laham, M. A.; Peng, C. Y.; Nanayakkara, A.; Challacombe, M.; Gill, P. M. W.; Johnson, B.; Chen, W.; Wong, M. W.; Gonzalez, C.; Pople, J. A. *Gaussian 03*, revision C.02; Gaussian, Inc.: Wallingford, CT, 2004.

(19) Peng, C.; Ayala, P. Y.; Schlegel, H. B.; Frisch, M. J. *J. Comput. Chem.* **1996**, *17*, 49–56.

(20) McLean, A. D.; Chandler, G. S. *J. Chem. Phys.* **1980**, *72*, 5639–5648.

(21) Sousa, S. P.; Fernandes, S. A.; Ramos, M. J. *J. Phys. Chem. A* **2007**, *111*, 10439–10452.

(22) (a) Becke, A. D. *J. Chem. Phys.* **1993**, *98*, 1372–1377. (b) Lee, C.; Yang, W.; Parr, R. G. *Phys. Rev. B* **1988**, *37*, 785–789.

(23) Barone, V.; Adamo, C. *J. Chem. Phys.* **1996**, *105*, 11007–11019.

(24) Lynch, B. J.; Zhao, Y.; Truhlar, D. G. *J. Phys. Chem. A* **2003**, *107*, 1384–1388.

(25) Dahlke, E. E.; Orthmeyer, M. A.; Truhlar, D. G. *J. Phys. Chem. B* **2008**, *112*, 2372–2381.

(26) (a) Dunning, T. H. *J. Chem. Phys.* **1989**, *90*, 1007–1023. (b) Woon, D. E.; Dunning, T. H. *J. Chem. Phys.* **1993**, *98*, 1358–1371.

(27) Cramer J. C. *Essentials of Computational Chemistry: Theories and Models*, 2nd ed.; John Wiley and Sons: New York, 2004.

(28) Rappe, A. K.; Bernstein, E. R. *J. Phys. Chem. A* **2000**, *104*, 6117–6128.

(29) Zhao, Y.; Truhlar, D. G. *J. Chem. Theory Comput.* **2005**, *1*, 415–432.

(30) Salvador, P.; Szczesniak, M. M. *J. Chem. Phys.* **2003**, *118*, 537–549.

(31) Kobko, N.; Dannenberg, J. J. *J. Phys. Chem. A* **2001**, *105*, 1944–1950.

(32) Pauling, L. *The Nature of the Chemical Bond*, 3rd ed.; Cornell University Press: Ithaca, NY, 1960.

(33) Dinescu, A.; Whiteley, C.; Combs, R. R.; Cundari, T. R. *J. Phys. Chem. A* **2006**, *110*, 4053–4056.

(34) Paizs, B.; Suhai, S. *J. Comput. Chem.* **1998**, *19*, 575–584.

(35) Wieczorek, R.; Haskamp, L.; Dannenberg, J. J. *J. Phys. Chem. A* **2004**, *108*, 6713–6723.

(36) Koné, M.; Illien, B.; Graton, J.; Laurence, C. *J. Phys. Chem. A* **2005**, *109*, 11907–11913.

(37) (a) Kozack, R. E.; Jordan, P. C. *J. Chem. Phys.* **1992**, *196*, 3131–3136. (b) Schmitt, U. W.; Voth, G. A. *J. Phys. Chem. B* **1998**, *102*, 5547–5551. (c) Ojamäe, L.; Shavitt, I.; Singer, S. J. *J. Phys. Chem.* **1998**, *109*, 5547–5564. (d) James, T.; Wales, D. J. *J. Chem. Phys.* **2005**, *122*, 134306(01)134306(11) .

(38) (a) Zhan, C.-G.; Dixon, D. A. *J. Phys. Chem. A* **2001**, *105*, 11534–11540. (b) Zhan, C.-G.; Dixon, D. A. *J. Phys. Chem. A* **2002**, *106*, 9737–9744. (c) Zhan, C.-G.; Dixon, D. A. *J. Phys. Chem. A* **2004**, *108*, 2020–2029.

JP806568K